The Astrophysical Journal, 733:50 (9pp), 2011 May 20 doi:10.1088/0004-637X/733/1/50

YSOVAR: THE FIRST SENSITIVE, WIDE-AREA, MID-INFRARED PHOTOMETRIC MONITORING OF THE ORION NEBULA CLUSTER

M. Morales-Calderón[1], J. R. Stauffer[1], L. A. Hillenbrand[2], R. Gutermuth[3,4], I. Song[5], L. M. Rebull[1], P. Plavchan[6], J. M. Carpenter[2], B. A. Whitney[7], K. Covey[8,9,33,34], C. Alves de Oliveira[10], E. Winston[11], M. J. McCaughrean[11,12], J. Bouvier[13], S. Guieu[14], F. J. Vrba[15], J. Holtzman[16], F. Marchis[17,18], J. L. Hora[19], L. H. Wasserman[20], S. Terebey[21], T. Megeath[22], E. Guinan[23], J. Forbrich[19], N. Huélamo[24], P. Riviere-Marichalar[24], D. Barrado[24,25], K. Stapelfeldt[26], J. Hernández[27], L. E. Allen[28], D. R. Ardila[29], A. Bayo[14], F. Favata[12], D. James[30,31], M. Werner[26], and K. Wood[32]

[1] Spitzer Science Center, California Institute of Technology, Pasadena, CA 91125, USA; mariamc@ipac.caltech.edu
[2] Astronomy Department, California Institute of Technology, Pasadena, CA 91125, USA
[3] Five College Astronomy Department, Smith College, Northampton, MA 01063, USA
[4] Department of Astronomy, University of Massachusetts, Amherst, MA 01003, USA
[5] Department of Physics and Astronomy, University of Georgia, Athens, GA 30602, USA
[6] NASA Exoplanet Science Institute, California Institute of Technology, Pasadena, CA 91125, USA
[7] Space Science Institute, 4750 Walnut Street, Suite 205, Boulder, CO 80301, USA
[8] Department of Astronomy, Cornell University, 226 Space Sciences Building, Ithaca, NY 14853, USA
[9] Department of Astronomy, Boston University, Boston, MA 02215, USA
[10] Laboratoire d'Astrophysique de Grenoble, Observatoire de Grenoble, 38041 Grenoble Cedex 9, France
[11] Astrophysics Group, College of Engineering, Mathematics, and Physical Sciences, University of Exeter, UK
[12] European Space Agency, Research & Scientific Support Department, ESTEC, Noordwijk, The Netherlands
[13] UJF-Grenoble 1/CNRS-INSU, Institut de Planétologie et d'Astrophysique de Grenoble (IPAG) UMR 5274, Grenoble, F-38041, France
[14] European Southern Observatory, Alonso de Córdova 3107, Vitacura, Santiago, Chile
[15] U.S. Naval Observatory, Flagstaff Station, 10391 W. Naval Observatory Road, Flagstaff, AZ 86001-8521, USA
[16] New Mexico State University, Box 30001/MSC 4500, Las Cruces, NM 88003, USA
[17] Department of Astronomy, UC Berkeley, 601 Campbell Hall, Berkeley, CA 94720, USA
[18] SETI Institute, Carl Sagan Center, 189 N San Bernado Avenue, Mountain View, CA 94043, USA
[19] Harvard-Smithsonian Center of Astrophysics, 60 Garden Street, Cambridge, MA 02138, USA
[20] Lowell Observatory, 1400 West Mars Hill Road, Flagstaff, AZ 86001, USA
[21] Department of Physics and Astronomy, California State University at Los Angeles, Los Angeles, CA 90032, USA
[22] Department of Physics and Astronomy, The University of Toledo, 2801 West Bancroft Street, Toledo, OH 43606, USA
[23] Department of Astronomy and Astrophysics, Villanova University, Villanova, PA 19085, USA
[24] Centro de Astrobiología (INTA-CSIC), LAEFF, P.O. Box 78, E-28691 Villanueva de la Canada, Spain
[25] Calar Alto Observatory, Centro Astronómico Hispano Alemán, Almería, Spain
[26] Jet Propulsion Laboratory, California Institute of Technology, Pasadena, CA 91109, USA
[27] Centro de Investigaciones de Astronomía, Apdo. Postal 264, Mérida 5101-A, Venezuela
[28] National Optical Astronomy Observatory, 950 North Cherry Avenue, Tucson, AZ 85719, USA
[29] NASA Herschel Science Center, California Institute of Technology, Pasadena, CA 91125, USA
[30] Hoku Kea Observatory, Department of Physics & Astronomy, University of Hawaii at Hilo, Hilo, HI 96720, USA
[31] Cerro Tololo Inter-American Observatory, Casilla 603, La Serena, Chile
[32] School of Physics & Astronomy, University of St Andrews, North Haugh, St Andrews, Fife, KY16 9AD, UK
Received 2011 March 16; accepted 2011 March 16; published 2011 May 3

ABSTRACT

We present initial results from time-series imaging at infrared wavelengths of 0.9 deg^2 in the Orion Nebula Cluster (ONC). During Fall 2009 we obtained 81 epochs of *Spitzer* 3.6 and 4.5 μm data over 40 consecutive days. We extracted light curves with ∼3% photometric accuracy for ∼2000 ONC members ranging from several solar masses down to well below the hydrogen-burning mass limit. For many of the stars, we also have time-series photometry obtained at optical (I_c) and/or near-infrared (JK_s) wavelengths. Our data set can be mined to determine stellar rotation periods, identify new pre-main-sequence eclipsing binaries, search for new substellar Orion members, and help better determine the frequency of circumstellar disks as a function of stellar mass in the ONC. Our primary focus is the unique ability of 3.6 and 4.5 μm variability information to improve our understanding of inner disk processes and structure in the Class I and II young stellar objects (YSOs). In this paper, we provide a brief overview of the YSOVAR Orion data obtained in Fall 2009 and highlight our light curves for AA-Tau analogs—YSOs with narrow dips in flux, most probably due to disk density structures passing through our line of sight. Detailed follow-up observations are needed in order to better quantify the nature of the obscuring bodies and what this implies for the structure of the inner disks of YSOs.

Key words: circumstellar matter – open clusters and associations: individual (Orion) – stars: pre-main sequence – stars: protostars – stars: variables: general

Online-only material: machine-readable table

1. INTRODUCTION

The Orion star-forming region has been the subject of more low-mass young star variability studies than any other region. While Haro (1969), Herbig & Kameswara Rao (1972), and

[33] Hubble Fellow.
[34] Visiting Researcher.

Table 1
Summary of Observations

Telescope/Instrument	Filter	Start/End Dates	No. of Epochs	Central Coordinates (J2000)	Area (arcmin)	Exp. time/Epoch (s)
Spitzer/IRAC		2009 Oct 23–Dec 1	81	05:35:10−05:42:25	30 × 35	(10.4 & 0.4) × 4
Spitzer/IRAC		2009 Oct 23–Dec 1	81	05:36:06−05:16:22	5 × 25	(10.4 & 0.4) × 4
Spitzer/IRAC	[3.6], [4.5]	2009 Oct 23–Dec 1	81	05:35:21−04:49:47	30 × 35	(10.4 & 0.4) × 4
Spitzer/IRAC		2009 Oct 23–Dec 1	81	05:34:37−05:20:00	10 × 25	(10.4 & 0.4) × 4
Spitzer/IRAC		2009 Oct 23–Dec 1	81	05:35:24−05:17:32	20 × 25	1.2 × 20
UKIRT/WFCAM	J	2009 Oct 20–Dec 22	32	05:35:17−05:22:49	52 × 104	2 × 3
CFHT/WIRCam		2009 Oct 27–Nov 8	11	05:35:14−04:41:34		
CFHT/WIRCam		2009 Oct 27–Nov 8	11	05:35:14−05:02:14		
CFHT/WIRCam	J, K_s	2009 Oct 27–Nov 8	11	05:36:04−05:22:46	21 × 21	(5 × 2) × 7 (J), 5 × 7 (K_s)
CFHT/WIRCam		2009 Oct 27–Nov 8	11	05:34:26−05:22:46		
CFHT/WIRCam		2009 Oct 27–Nov 8	11	05:35:14−05:43:28		
NMSU APO1 m/CCD	I_c	2009 Oct 24–2010 Feb 9	27	05:35:18−05:24:03	15 × 15	60 × 20
SuperLotis/CCD	I_c	2009 Oct 28–Dec 12	23	05:35:11−05:41:02	16 × 16	180 × 12

Walker (1978) all conducted pioneering studies of the variability of young stars in Orion, the modern era using two-dimensional imaging cameras was initiated by Herbst and his team (Attridge & Herbst 1992; Choi & Herbst 1996). They obtained multi-year, optical time-series photometry of several regions of the Orion Nebula Cluster (ONC), eventually obtaining light curves for hundreds of pre-main-sequence (PMS) stars, often spanning several years. Those data were primarily used to derive rotation periods—made possible by the fact that the photospheres of young stars are often heavily spotted (cold and/or hot spots), resulting in flux variations modulated at the star's rotation period. Many other groups subsequently obtained time-series photometry of other portions of the ONC, using optical (Stassun et al. 1999; Rebull 2001; Herbst et al. 2002; Irwin et al. 2007) and near-IR (Carpenter et al. 2001) imaging data. In many cases, the light curve shapes are well fit by hot or cold spots, normally at moderately high latitudes since the light curves are seldom "flat-bottomed." However, for a significant fraction of the light curves, particularly those in the near-IR, spots do not seem to provide a good explanation of the observed variability (Carpenter et al. 2001).

Time-series photometry of young stellar objects (YSOs) can also address issues other than rotational velocities such as flares and flare frequency (Parsamian et al. 1993), disk instabilities (Fedele et al. 2007; Herbst et al. 2010; Plavchan et al. 2008a), and eclipsing binaries as tests of PMS isochrones (Stassun et al. 2004, 2006; Cargile et al. 2008). Mid-IR time-series photometry of YSOs could, in principle, detect variations in the temperature or spatial distribution of warm dust in the inner circumstellar disks of these stars, thereby informing models of disk evolution and perhaps of planet formation. We recently completed the first sensitive, wide-area, mid-IR time-series photometric monitoring program for the ONC using the Infrared Array Camera (IRAC; Fazio et al. 2004) on the *Spitzer Space Telescope* (Werner et al. 2004). We report here some early results from that program, with more detailed analysis of specific classes of variability to follow.

2. OBSERVATIONS

2.1. Spitzer Observations

Our GO6 Exploration Science program YSOVAR (Young Stellar Object Variability) provides the first large-scale survey of mid-IR photometric variability of YSOs. In Fall 2009, we used ∼250 hr of warm *Spitzer* observing time to monitor ∼0.9 deg^2 of the ONC at 3.6 and 4.5 μm.

The observed area was broken into five segments with a central region of $\sim 20' \times 25'$ and four flanking fields. The central part was observed in full array mode with 1.2 s exposure time and 20 dithering positions to avoid saturation by the bright nebulosity around the Trapezium stars. The remaining four segments of the map were observed in High Dynamic Range mode with exposure times of 10.4 and 0.4 s, and four dithering positions. A summary of the observations appears in Table 1.

These observations were taken for 40 days in Fall 2009, with ∼2 epochs each day but with an interval between observations that varied both by design (to reduce period-aliasing problems) and due to constraints imposed by other *Spitzer* programs that were executed during the same campaigns. We used the IDL package Cluster Grinder (Gutermuth et al. 2009) which, starting from the basic calibrated data (BCD) images released by the *Spitzer* Science Center, builds the combined mosaic for each epoch and performs aperture photometry on the mosaics. In the present work, the BCD images used correspond to the S18.12 software build (the zero point magnitudes are 19.30 and 18.67 for 1 DN s^{-1} total flux at 3.6 and 4.5 μm, respectively). Future versions of the pipeline will include improvements, most importantly using better linearity corrections.

2.2. Ground-based Data

In order to complement our *Spitzer* data, we also obtained I_c, J, and K_s contemporaneous photometry, usually for smaller areas within the *Spitzer* mosaic. The main data sets come from the UKIRT Wide Field Camera (WFCAM), the Canada–France–Hawaii Telescope (CFHT) Wide Field Infrared Camera (WIRCam), the Steward Observatory Super-LOTIS (Livermore Optical Transient Imaging System) robotic telescope, and the NMSU/APO 1 m telescope. A summary of the principal characteristics of each data set appears in Table 1. A deeper discussion on data reduction of this data set plus additional data collected for this project will be described in R. Gutermuth et al. (2011, in preparation).

We performed differential aperture photometry on the ground-based data. In each data set, for each object, an artificial reference level was created by selecting 30 nearby isolated stars; we iteratively eliminated those with larger photometric scatter or evidence of variability. Finally, the time series are incorporated into a database publicly available at http://ysovar.ipac.caltech.edu/. This data release includes a color image of the surveyed field of view, fits files for the 3.6 and 4.5 μm mosaics from a single epoch, a table for all ONC stars

Table 2
Time Series at the [3.6] and [4.5] IRAC Bands for the ONC Stars

Object	MJD (days)	IRAC Band	Mag	Error	R.A. J2000 (deg)	Decl. J2000 (deg)
ISOY_J053532.71−045011.9	55127.50781250	IRAC1	8.725	0.006	83.886268	−4.836648
ISOY_J053532.71−045011.9	55127.76562500	IRAC1	8.715	0.006	83.886268	−4.836648
ISOY_J053532.71−045011.9	55128.00781250	IRAC1	8.704	0.006	83.886268	−4.836648
ISOY_J053532.71−045011.9	55128.37890625	IRAC1	8.741	0.004	83.886268	−4.836648
ISOY_J053532.71−045011.9	55128.76171875	IRAC1	8.814	0.006	83.886268	−4.836648
ISOY_J053532.71−045011.9	55129.25781250	IRAC1	8.795	0.005	83.886268	−4.836648
ISOY_J053532.71−045011.9	55129.89843750	IRAC1	8.823	0.006	83.886268	−4.836648
ISOY_J053532.71−045011.9	55130.69921875	IRAC1	8.905	0.005	83.886268	−4.836648
ISOY_J053532.71−045011.9	55131.35937500	IRAC1	8.925	0.007	83.886268	−4.836648
ISOY_J053532.71−045011.9	55131.58593750	IRAC1	8.912	0.006	83.886268	−4.836648

(This table is available in its entirety in a machine-readable form in the online journal. A portion is shown here for guidance regarding its form and content.)

providing the name, aliases, R.A., decl., *J*, *H*, *K*, [3.6], [4.5], [5.8], [8.0], and [24] information as in T. Megeath et al. (2011, in preparation), a file with plots of multi-wavelength light curves, and the actual time series for all ONC members either as ASCII files or by querying the database. Alternatively, the time series can be found in Table 2.

3. VARIABILITY STATISTICS AND TYPES

Light curves were extracted in both IRAC bands for 1249 Class I and II previously known Orion YSOs with IR excess (T. Megeath et al. 2011, in preparation) and inferred masses between 0.03 and ∼2 $M_{\odot}$, plus 820 other likely Orion members. This latter set of objects is formed by sources that fulfill at least one of the following conditions: (1) has been labeled as a member by proper motion studies such as Parenago (1954), Jones & Walker (1988), McNamara (1976), and Tian et al. (1996), (2) has been labeled as a member according to Hillenbrand et al. (1998), (3) has been labeled as a member by X-ray studies (Getman et al. 2005), (4) has H_{α} profiles typical of weak-lined T Tauris (WTTs; Tobin et al. 2009; Fűrész et al. 2008), (5) has been labeled as variable by Carpenter et al. (2001), or (6) finally, we have included all the sources that have been claimed to be periodic variables. Most of these stars are WTTs according to the Megeath et al. photometry, though some may be sources with excesses that escaped previous detection. In addition to these 2069 Orion stars, another 147 Class I and Class II sources plus 209 Orion members without IR excess have light curves in just one of the two IRAC bands.

We estimated the noise in the IRAC light curves by measuring the typical scatter for all the objects in the field. In that way, we estimate a relative per channel photometric accuracy better than 3% down to [3.6] = 14 and better than 10% for objects as faint as [3.6] = 16. For the *J* band, we derive accuracies of ∼2% down to *J* = 16.5 and of ∼10% to *J* = 18.5 for the ensemble. Note that the accuracy varies significantly over the surveyed field due to nebular emission.

Approximately 70% of the YSOs with IR excess are variable based primarily on the Stetson index calculated using both IRAC channels together (Welch & Stetson 1993; see Table 3 for statistics). The variable sources were visually inspected and, in addition to the Stetson variables, we considered as variables as well a few YSOs for which a period could be found even when the Stetson index alone would not reflect the variability. About 3% of the variable YSOs have been selected in this way. Usually these sources have very low amplitude; however, most of them have previously detected periods that match the ones derived here and thus we believe the variability is real. The variable stars exhibit diverse behavior with time, including slow drifts in brightness over one month or longer that may be caused by a slow change in accretion rate or by self-shadowing in a warped disk (Figure 1(a)), rapid chaotic flux variations probably caused by changes in the accretion geometry (Figure 1(b)), flares (Figure 1(c)), stars with light curves that look "periodic" for part but not all of the 40 day period or for which the periodic variations are mixed with other longer term changes (Figure 1(d)), periodic or pseudo-periodic variations arising from photospheric spots and/or disk warps (Figure 1(e)), changes in color that may be produced by variable extinction (Figure 1(f)), and stars that show narrow or broad dips in the observed flux superimposed on an otherwise nearly constant flux level (see the following section).

Table 3
Statistics

Sample	Class I	Class II	Class III
No. of sources	126	1123	820
IRAC variables	106	787	366
Variables w/[3.6] amp. >0.2 mag	71	465	92
Variables w/[3.6] amp. >0.5 mag	15	59	8
Variables w/[3.6] amp. >1 mag	3	1	0
[3.6] − [4.5] Color variables w/amp. >0.2 mag	3	5	0
Prev. known periods	8	266	334
Recovered periods	5	125	189
New periods	8	76	98
No. of AA-Tau analogs	1	37	3

Figure 2 illustrates the value of having contemporaneous optical/NIR/mid-IR monitoring (12%, 85%, and 37% of the Orion stars have K_s-, *J*-, and I_c-band light curves, respectively). When compared to the near-IR and optical data, the mid-IR light curves usually have similar shapes. We have derived the amplitude of the light curves at each band as the difference between the maximum and minimum values of the magnitude at that bandpass avoiding single deviant data points. There are generally larger amplitudes at shorter wavelengths (∼60% of the variables with shorter wavelength data—Figure 2(a)), though in some cases, the amplitudes of variation are similar at all bands (∼30% of the variables with shorter wavelength data—Figure 2(b)). In a small number of cases, the IRAC variations are smaller or non-apparent at shorter wavelengths, indicating that the source of variability is probably in the disk (∼10% of the variables with shorter wavelength data—Figures 2(c) and (d)). In only two cases do we find a phase

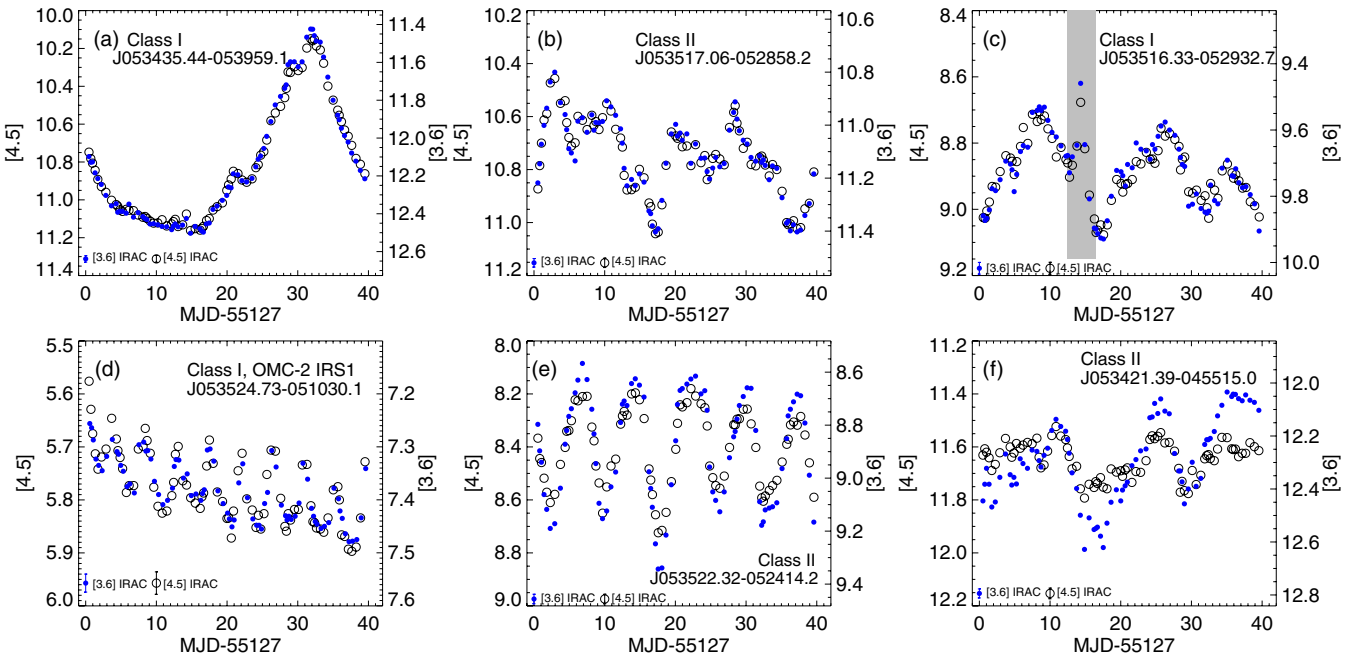

Figure 1. Sample IRAC light curves for several stars showing the range of different variability types found in our data: (a) slow drifts in brightness that may be caused by a slow change in accretion rate or by self-shadowing in a warped disk, (b) rapid chaotic flux variations probably caused by changes in the accretion geometry, (c) flares, (d) periodic variations mixed with other longer term changes, (e) periodic variations arising from photospheric spots and/or disk warps, (f) changes in color that may be produced by variable extinction. The symbols are •: [3.6]; ○: [4.5]. [3.6] and [4.5] magnitudes have been plotted on the right and left vertical axes, respectively.

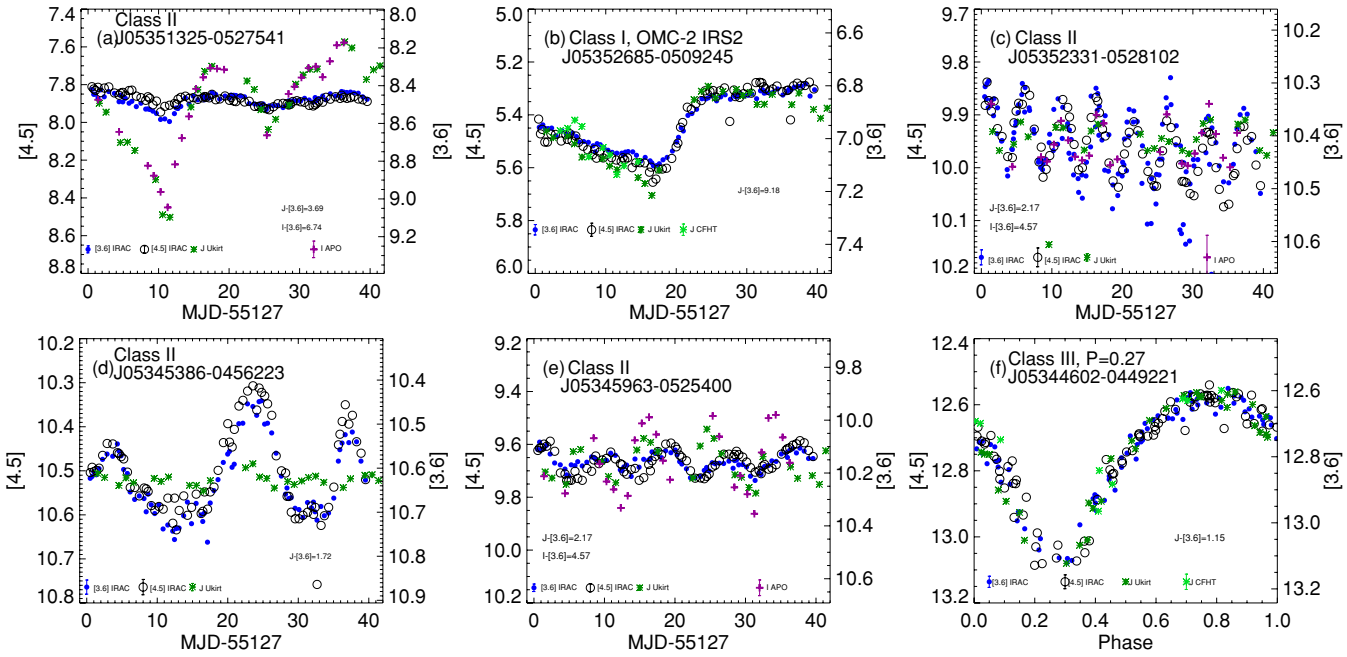

Figure 2. Sample light curves for several stars showing shorter wavelength ground-based as well as *Spitzer* data selected to display the different variability types found in our data: (a) larger amplitudes at shorter wavelengths, (b) similar amplitudes of variation at all wavelengths, (c) larger IRAC amplitudes than the shorter wavelength amplitudes, (d) IRAC variations that are non-apparent at shorter wavelengths, (e) difference in phase between the optical and near-IR data relative to IRAC data. Panel (f) shows the phased light curve of star 1165 of Stassun et al. (1999). The symbols are •: [3.6]; ○: [4.5]; ∗: *J* (dark green: UKIRT, light green: CFHT); and +: I_c. [3.6] and [4.5] magnitudes have been plotted on the right and left vertical axes, respectively. I_c and *J* light curves have been shifted on the *y*-axis to match the mean IRAC values. The amount shifted is stated in each panel.

difference between the optical and near-IR data relative to IRAC data (Figure 2(e)). Some of these effects can be explained by the presence of one or more hot spots on the surface of the star and/or the existence of warps in its disk.

Several of the objects deserve particular mention. Figure 1(d) shows the well-known intermediate-mass protostar OMC-2 IRS 1, for which outflows have been detected (Yu et al. 1997; Reipurth et al. 1999; Takahashi et al. 2008; Anathpindika & Whitworth 2008); a similar light curve was previously reported for Orion BN/KL (J053514.12−052222.9; Hillenbrand et al. 2001), though the physical mechanism for such variability in these B-type (Johnson et al. 1990; Hillenbrand et al. 2001) YSOs is not obvious. In Figure 2(b), we show the protostar OMC-2 IRS 2, which has also been associated with a jet (Yu

et al. 1997; Anathpindika & Whitworth 2008) but for which only one scattering lobe is seen, suggesting that its disk is significantly less inclined to the line of sight (Rayner et al. 1989). Figure 2(f) shows the light curve of a star identified by Stassun et al. (1999) as the fastest rotator in a study of the period distribution in the ONC ($P = 0.27$ days, Star 1161 of Stassun et al. 1999; R.A. 05 34 45.93, decl. −04 49 22.0, from his Table 1). Given its spectral type (K5; Rebull 2001), at 1–2 Myr, this period is shorter than breakup. However, the VI_cJHK photometry for the star suggests an age older than 30 Myr if it is at Orion distance. Because the light curve in Stassun et al. appears to have identical shape and amplitude to our 2009 light curve, we suspect this object is a tidally distorted binary, but it could also be a single near zero-age main-sequence rapid rotator (similar to H II 1883 in the Pleiades).

In general, our variable YSOs show colorless changes at IRAC bands (∼88% of our sample shows IRAC [3.6]−[4.5] rms amplitudes smaller than 0.05 mag). The objects that do show IRAC color variations usually become redder as they fade. The typical peak-to-peak amplitudes in each IRAC band are ∼0.2 mag. The most extreme stars in our sample have changes in amplitude as large as ∼1.8 mag and the largest change in color is ∼0.3 mag.

We have used the NStED Periodogram Service[35] to derive periods for our sample. This service uses the Lomb–Scargle (Scargle 1982), Box-fitting Least Squares (Kovács et al. 2002), and Plavchan (Plavchan et al. 2008b) algorithms for computing periodograms from time-series data. Given the cadence of our data, the periodograms are formally reliable for periods between 1 and 40 days; however, we have found 11 sources with periods shorter than a day. Those sources all have periods from the literature that match our determinations and the light curves are so well phased that we believe the periods are real. We have not retained any period longer than 25 days. In this way we can determine a period for 23% of the variable YSOs with IR excess; 7% of these are Class Is and 93% are Class IIs. Among the non-excess sources, ∼44% are variables and the predominant variability is periodic, probably due to photospheric spots; 33% of the WTTs have periods discernible from the *Spitzer* data. In the total ONC sample (1249 *Spitzer* excess sources plus 820 Orion members not known to have IR excess), we find 150 new periods (see Table 4). About 30% of our total sample had previously published periods. Of these, we recover the published period for 57% of the WTTs and 47% for the YSOs with IR excess. This difference is likely due to the thermal emission from dust at IRAC wavelengths significantly degrading the sensitivity to photospheric phenomena but also because the stars themselves may change (Rebull 2001).

Finally, we have identified nine eclipsing binaries in our sample. Four of them, 2MASS 05352184−0546085 (Stassun et al. 2006), V1174 Ori (Stassun et al. 2004), Par1802 (Cargile et al. 2008), and JW 380 (Irwin et al. 2007) are already known. A fifth one, Theta 1 Ori E, is a known spectroscopic binary (Herbig & Griffin 2006; Costero et al. 2008) which was flagged as potentially eclipsing, but no confirmatory photometry had been obtained until now. We are working to obtain spectroscopic confirmation of the four new eclipsing binary candidates and will report on their status in a future paper. Their coordinates and tentative periods can be found in Table 5.

[35] http://nsted.ipac.caltech.edu/periodogram/cgi-bin/Periodogram/nph-simpleupload

Table 4
New Periods for Orion Members

Source[a]	Period (days)	p-value[b]
ISOY_J053427.70−053155.4	3.37	4.78E−4
ISOY_J053434.88−044243.5	9.36	1.31E−4
ISOY_J053435.15−053210.4	5.18	2.46E−5
ISOY_J053435.98−045218.0	2.34	2.80E−3
ISOY_J053439.11−053839.2	2.41	3.01E−2
ISOY_J053439.76−052425.6	16.97	1.65E−4
ISOY_J053441.18−054611.7	8.02	1.18E−3
ISOY_J053441.71−052653.0	8.47	9.13E−2
ISOY_J053441.87−055502.6	1.66	3.23E−6
ISOY_J053442.74−052837.6	6.15	1.40E−7
ISOY_J053445.00−045559.2	3.40	3.60E−3
ISOY_J053447.64−054350.7	4.27	1.35E−2
ISOY_J053447.74−052632.1	1.84	5.73E−6
ISOY_J053447.85−044228.9	8.36	8.55E−4
ISOY_J053449.57−052903.4	14.73	9.90E−7
ISOY_J053450.66−050407.7	9.24	2.03E−3
ISOY_J053450.72−045836.8	6.32	3.80E−7
ISOY_J053452.22−045102.7	5.15	1.52E−2
ISOY_J053452.49−044940.4	6.25	5.78E−2
ISOY_J053452.60−051536.6	2.35	3.00E−7
ISOY_J053453.12−055955.0	2.55	3.09E−2
ISOY_J053453.99−044537.3	2.38	1.00E−8
ISOY_J053454.83−052512.6	3.75	2.88E−4
ISOY_J053454.90−054643.9	13.55	4.70E−7
ISOY_J053454.92−050128.4	13.90	2.89E−2
ISOY_J053457.20−050823.9	1.63	2.85E−5
ISOY_J053458.53−060000.4	5.98	6.03E−2
ISOY_J053500.22−052409.2	7.29	2.60E−4
ISOY_J053500.54−054859.1	6.63	9.01E−6
ISOY_J053501.08−052304.1	3.98	6.39E−5
ISOY_J053501.10−052337.3	7.12	4.55E−3
ISOY_J053501.34−052811.9	7.23	7.00E−8
ISOY_J053501.34−054113.5	8.41	1.36E−5
ISOY_J053502.38−051548.0	6.09	1.49E−6
ISOY_J053503.12−050917.0	4.32	5.17E−5
ISOY_J053503.24−051726.4	4.73	5.13E−6
ISOY_J053503.70−052245.7	5.11	1.00E−8
ISOY_J053504.56−052013.9	8.43	1.40E−7
ISOY_J053504.61−045829.0	4.67	1.04E−3
ISOY_J053504.80−060020.8	5.13	1.83E−3
ISOY_J053504.95−052109.2	10.12	2.00E−8
ISOY_J053505.45−052230.5	3.56	2.25E−4
ISOY_J053505.71−052354.1	20.48	5.41E−1
ISOY_J053505.79−053827.8	2.80	3.50E−7
ISOY_J053505.85−044843.3	6.16	1.63E−2
ISOY_J053506.77−055101.3	6.76	1.50E−4
ISOY_J053506.86−051133.2	5.47	1.04E−6
ISOY_J053507.01−050134.8	2.83	8.27E−3
ISOY_J053507.70−055749.5	3.75	3.89E−2
ISOY_J053508.02−053244.3	6.87	2.13E−4
ISOY_J053508.07−054853.8	7.97	2.78E−4
ISOY_J053508.26−055000.3	6.83	1.04E−6
ISOY_J053509.95−051449.9	2.19	8.94E−6
ISOY_J053510.02−051816.6	9.37	1.00E−8
ISOY_J053510.99−051521.8	11.29	3.53E−3
ISOY_J053511.10−051601.8	4.75	2.00E−8
ISOY_J053511.48−052352.0	22.37	1.49E−2
ISOY_J053511.56−052448.0	3.74	7.68E−2
ISOY_J053511.62−051912.3	6.77	2.36E−2
ISOY_J053511.89−052002.0	4.66	1.40E−6
ISOY_J053511.95−052845.0	3.11	1.13E−4
ISOY_J053513.46−053502.8	7.28	9.36E−4
ISOY_J053513.57−053508.1	5.73	3.24E−2
ISOY_J053514.66−050312.6	7.66	2.28E−4
ISOY_J053514.88−055142.2	4.27	6.33E−4
ISOY_J053515.48−052722.7	6.54	2.84E−6

Table 4
(Continued)

Source[a]	Period (days)	p-value[b]
ISOY_J053515.49−053511.9	5.76	3.71E−2
ISOY_J053515.52−055316.2	10.43	6.00E−8
ISOY_J053515.56−045308.1	13.22	3.90E−7
ISOY_J053515.65−055214.6	8.67	3.49E−4
ISOY_J053515.76−052309.9	9.90	3.00E−8
ISOY_J053516.33−052932.7	16.79	3.08E−6
ISOY_J053516.98−053246.4	3.77	1.42E−2
ISOY_J053517.10−051900.8	17.46	2.17E−3
ISOY_J053517.21−044113.6	1.05	6.44E−2
ISOY_J053517.35−052235.8	7.10	2.35E−2
ISOY_J053517.40−045957.2	3.00	9.60E−2
ISOY_J053517.53−051929.0	6.72	2.48E−5
ISOY_J053517.54−051613.1	4.06	7.10E−7
ISOY_J053517.97−054937.5	6.27	5.94E−2
ISOY_J053518.03−052205.4	5.63	1.06E−5
ISOY_J053518.23−051745.0	3.28	4.39E−6
ISOY_J053518.29−050805.0	4.85	2.71E−4
ISOY_J053518.70−051801.8	7.37	1.97E−4
ISOY_J053519.86−053103.8	4.23	6.85E−6
ISOY_J053520.02−052911.9	2.79	1.37E−2
ISOY_J053520.06−050358.5	12.41	9.96E−4
ISOY_J053520.19−052308.6	9.02	3.32E−3
ISOY_J053520.29−054639.9	7.90	5.73E−2
ISOY_J053520.72−051926.5	22.21	1.00E−8
ISOY_J053521.38−050942.3	3.76	9.00E−8
ISOY_J053521.62−052325.8	13.72	3.39E−5
ISOY_J053522.10−051857.6	5.78	8.76E−6
ISOY_J053522.32−044133.3	10.29	9.60E−2
ISOY_J053522.73−051838.2	5.75	5.20E−7
ISOY_J053522.98−051521.8	4.32	1.33E−3
ISOY_J053523.04−052941.5	2.94	1.30E−7
ISOY_J053523.18−052228.3	8.33	5.18E−3
ISOY_J053523.97−055942.0	18.70	7.13E−5
ISOY_J053524.33−050120.5	14.65	1.23E−4
ISOY_J053524.34−052232.3	18.91	3.02E−6
ISOY_J053524.62−052104.2	16.78	7.10E−3
ISOY_J053524.67−044943.0	17.15	9.00E−7
ISOY_J053524.73−051030.1	4.37	3.47E−4
ISOY_J053525.18−050509.3	5.64	9.42E−5
ISOY_J053526.06−052121.0	2.58	1.28E−4
ISOY_J053526.47−053016.4	3.70	4.34E−5
ISOY_J053526.88−044730.7	3.91	3.07E−5
ISOY_J053527.00−054845.8	11.27	4.94E−2
ISOY_J053527.27−050527.0	17.86	6.35E−3
ISOY_J053527.66−054255.1	12.31	6.22E−4
ISOY_J053528.19−050341.2	23.52	3.48E−5
ISOY_J053529.65−052002.2	2.44	4.66E−6
ISOY_J053530.61−045936.1	8.57	3.05E−4
ISOY_J053532.67−054528.4	2.53	6.30E−7
ISOY_J053532.71−045011.9	14.38	4.32E−6
ISOY_J053532.96−051204.7	1.30	1.35E−4
ISOY_J053533.34−051145.6	16.19	1.40E−7
ISOY_J053533.60−052209.8	21.48	1.20E−7
ISOY_J053534.03−055505.8	11.47	1.04E−4
ISOY_J053535.16−051946.9	4.12	1.12E−2
ISOY_J053535.22−044739.6	10.24	3.88E−2
ISOY_J053536.49−044259.2	2.46	2.34E−2
ISOY_J053536.50−052009.4	9.87	3.97E−4
ISOY_J053538.56−050803.4	16.77	3.49E−6
ISOY_J053539.07−052025.7	4.51	1.82E−2
ISOY_J053539.49−044019.3	3.31	3.53E−3
ISOY_J053539.74−045141.7	3.05	6.27E−7
ISOY_J053539.77−044024.3	17.91	6.18E−3
ISOY_J053540.15−053723.7	6.31	4.05E−2
ISOY_J053541.70−052014.9	6.67	1.72E−2
ISOY_J053541.79−045027.7	24.80	1.26E−3

Table 4
(Continued)

Source[a]	Period (days)	p-value[b]
ISOY_J053542.01−051011.5	8.21	6.91E−4
ISOY_J053544.09−050837.6	4.46	1.40E−7
ISOY_J053545.32−044334.9	2.36	4.33E−2
ISOY_J053546.23−051808.6	9.71	2.00E−8
ISOY_J053547.80−051030.8	2.26	2.47E−6
ISOY_J053551.07−051508.9	9.36	4.56E−5
ISOY_J053552.10−044915.1	3.76	9.46E−4
ISOY_J053553.21−044734.7	1.73	2.99E−2
ISOY_J053554.63−052707.5	8.45	6.27E−7
ISOY_J053556.10−052533.0	5.17	2.46E−5
ISOY_J053558.94−053253.9	8.31	8.38E−4
ISOY_J053559.17−053552.7	19.04	1.54E−3
ISOY_J053605.95−050041.2	3.56	6,04E−3
ISOY_J053606.67−045512.1	1.66	1.01E−4
ISOY_J053606.99−051334.2	2.65	5.66E−6
ISOY_J053609.28−045000.8	15.16	1.07E−2
ISOY_J053612.32−045819.0	4.09	9.61E−2
ISOY_J053614.94−051533.7	4.72	4.05E−3

Notes.
[a] ISOY stands for Initial *Spitzer* Orion YSO.
[b] The p-value is the probability of chance occurrence returned by the periodogram service.

Table 5
New PMS Eclipsing Binary Candidates

Source[a]	Period (days)
ISOY_J053526.88−044730.7	3.91
ISOY_J053518.03−052205.4	5.63
ISOY_J053505.71−052354.1	20.39
ISOY_J053605.95−050041.2	3.56

Note. [a] ISOY stands for Initial *Spitzer* Orion YSO.

4. "DIPPER" OBJECTS: CLOUDS IN THE DISK?

4.1. Identification and Characterization

One of the most surprising and interesting classes of variability we find is narrow flux dips. This subset of 41 variables shows brief, sharp drops in their flux density with durations of one to a few days. These objects are members of the "Type III" variable class identified by Herbst et al. (1994) based on an optical synoptic data set; their most famous prototype is AA Tau (Bouvier et al. 2003). A few examples of such "dipper" light curves are shown in Figure 3. Among the identified cases, some exhibit only one dip, but typically >1 dip is seen over the 40 days. Periodic dips are also detected in about a third of these objects, with periods from $\sim$2 to 14 days. The dip amplitude is typically several tenths of a magnitude in the IRAC bands and ranges from 0.16 to 1.5 mag at *J*.

The criteria imposed for selecting dipper stars were (1) a distinctive dip extends over several IRAC epochs unless a single epoch IRAC dip is corroborated by the independent but contemporaneous shorter wavelength data. Implicitly, this means the IRAC-only dips will be broader in time, on average, than dips where shorter wavelength data confirm the dip. (2) If based on just an apparent dip in one IRAC epoch, both IRAC channels must agree and the I_c- or *J*-band data must show a larger amplitude dip by at least 50% to avoid misidentification of eclipsing binary stars as AA-Tau analogs. (3) The "continuum" must be flat enough so that the IRAC dip "stands out." Although

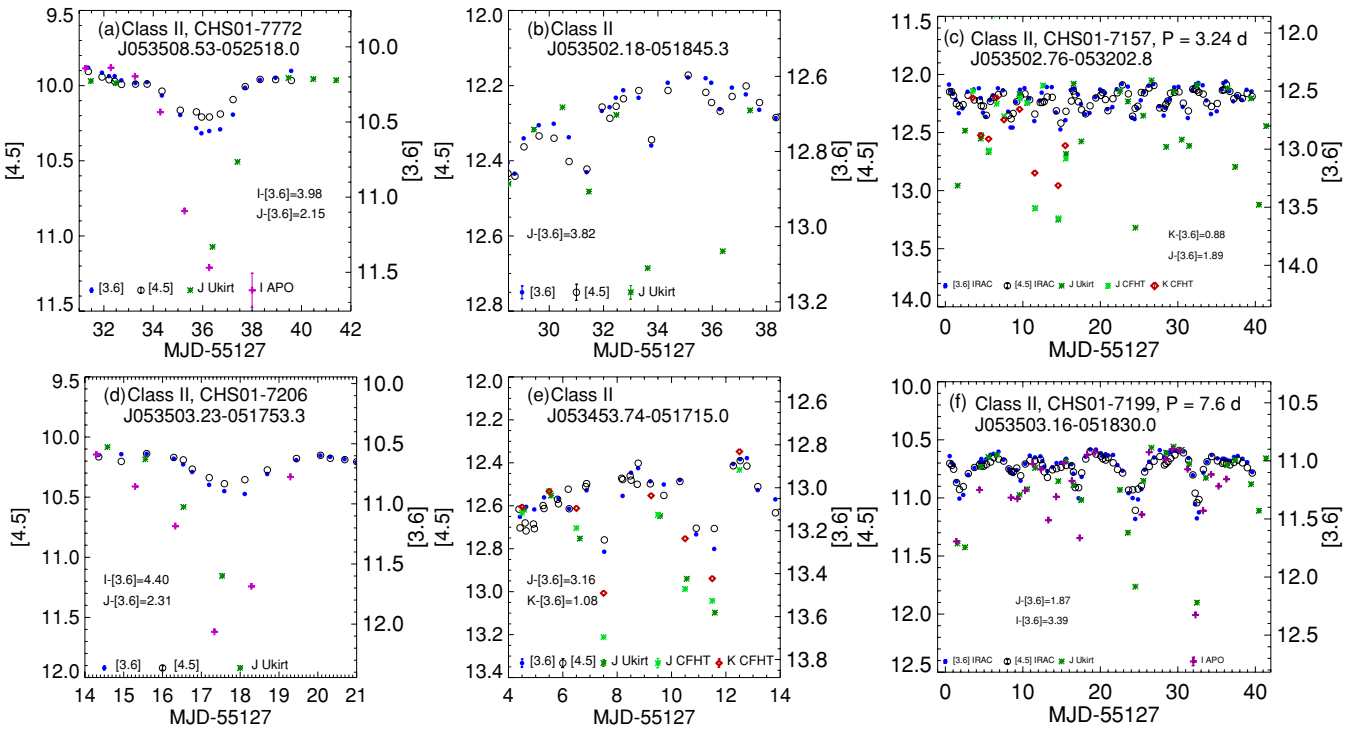

Figure 3. Sample light curves for six of the stars showing flux dips that can be discerned against a steady or slowly varying continuum. The two leftmost objects show broad dips that are not repeated over the duration of the observation. The two central panels show two of the narrowest dips and the two rightmost sources show periodic dips. The symbols are •: [3.6]; ○: [4.5]; ◇: K_s; ∗: J (dark green: UKIRT, light green: CFHT); and +: I_c (pink: SLOTIS, purple: APO). [3.6] and [4.5] magnitudes have been plotted on the right and left vertical axes, respectively. I_c, J, and K_s light curves have been shifted on the y-axis to match the mean IRAC values. The amount shifted is stated in each panel.

their identification by eye is generally straightforward, it is not as straightforward to determine the frequency of such dips in the overall data set. To do so, one must account for the likely superposition of such events with other types of variability that are occurring in the same stars. The optical and near-IR data were obtained at intervals of one to a few days as compared with the IRAC data which were obtained at half-day intervals, thus preventing confirmation of some IRAC dips. To detect these events requires good signal-to-noise ratio (S/N) data in all the relevant bandpasses, which eliminates many of the fainter stars and/or stars in regions where the nebular background is bright or very structured.

Based on the above criteria, we identify 38 of the Class I or II YSOs as having one or more AA-Tau-like flux dips. Given the coverage, cadence, and S/N that we have in different filters, we estimate that we would be able to identify ∼70% of broad dips (Figures 3(a) and (d)) and about 40% of the narrow dips (those present in just one IRAC epoch, Figures 3(b) and (e)). Thus, at present, we estimate the overall frequency of dipper stars at ∼5% or higher. We note that this fraction is much lower than the 28% estimated by Alencar et al. (2010) for periodic "AA-Tau-like" behavior in optical wavelength *CoRoT* data among a smaller set of young stars in NGC 2264. There are, in fact, a variety of reasons that *CoRoT* detects a larger fraction of "dipper" sources in NGC 2264 than the *Spitzer* YSOVAR survey of the ONC: *CoRoT*'s much better relative photometric accuracy (<1 mmag) and higher cadence (every 512 s during 23 days of uninterrupted observations), the larger amplitude of these dips at shorter wavelengths, the selection criteria itself, and the greater complexity of the mid-IR light curves due to the disk contribution. However, there may also be some real difference between the YSOs in the two clusters. Examination of the Carpenter et al. (2001) monitoring NIR data reveals that ∼50% of our dippers displayed similar behavior 10 years ago, suggesting some stability in physical mechanism inducing the variations. We have identified 13 objects, or 34% of the "dipper" sample, as being periodic with $P < 40$ days (the observing window). Carpenter et al. (2001) derived similar periods (less than 0.6 days of difference and usually less than 0.1 days) for five of these objects. The dependence of depth on wavelength is roughly consistent with that expected for the standard extinction law, as previously reported for AA Tau (Bouvier et al. 2003). Coordinates, periods, and amplitudes for the dippers can be found in Table 6.

Considering other existing data for our ONC stars, specifically the *Spitzer* photometry including all IRAC bands and MIPS 24 μm, Two Micron All Sky Survey (2MASS) near-infrared, and literature optical photometry and spectral types, we find that there is no clear distinction of the AA-Tau analogs in either *Spitzer*/IRAC or 2MASS magnitudes and colors relative to the rest of the ONC population, other than these objects are most often associated with Class II type YSOs. Only one of the 129 Class Is versus 37 of the 1175 Class IIs are identified as AA-Tau analogs.

4.2. Interpretation

The AA-Tau variability phenomenon has been interpreted (Bertout 2000; Bouvier et al. 2003) as arising from the rotation of a circumstellar disk with a high latitude "warp" that periodically obscures the star in addition to the extinction due to a flared disk that is typically imposed over the rest of the orbit. However, any process which creates overdense asymmetric regions in the inner disk could produce the flux dips.

Table 6
ONC AA-Tau Analogs

Source[a]	Mean I (mag)	Mean J (mag)	Mean [3.6] (mag)	Mean [4.5] (mag)	Dip Depth I[b] (mag)	Dip Depth J[b] (mag)	Dip Depth [3.6][b] (mag)	Dip Depth [4.5][b] (mag)	Dip Period (days)
ISOY_053432.02−052742.7	...	13.255	10.437	10.015	...	0.7	0.2	0.17	...
ISOY_053435.98−045218.0	...	13.972	12.131	11.754	...	0.6	0.2	0.15	2.34 ± 0.12
ISOY_053440.64−050658.7	...	13.989	10.509	10.136	...	1.1	0.5	0.38	3.85 ± 0.39
ISOY_053446.79−052129.2	...	13.424	11.213	10.862	...	0.42	0.25	0.20	...
ISOY_053450.72−045836.8	...	12.147	10.193	9.968	...	0.34	0.20	0.26	6.32 ± 0.38
ISOY_053450.87−053929.2	14.319	12.623	10.688	10.35	...	0.20	0.12	0.10	...
ISOY_053453.74−051715.0	...	16.316	13.158	12.675	...	0.7	0.45	0.34	...
ISOY_053455.10−044941.5	...	13.253	11.09	10.749	...	0.85	0.27	0.18	...
ISOY_053502.18−051845.3	...	16.589	12.772	12.347	...	0.45	0.16	0.13	...
ISOY_053502.76−053202.8	...	14.451	12.566	12.217	...	1.1	0.35	0.25	3.24 ± 0.78
ISOY_053503.16−051830.0	14.424	12.904	11.038	10.736	1.35	1.25	0.58	0.45	7.57 ± 0.72
ISOY_053503.23−051753.3	15.098	13.002	10.696	10.252	1.40	1.15	0.35	0.25	...
ISOY_053503.96−051859.8	15.105	13.069	10.841	10.423	0.95	0.60	0.40	0.35	...
ISOY_053504.68−044621.9	...	15.488	11.697	11.148	...	1.55	0.6	0.5	...
ISOY_053504.86−054426.7	18.038	15.385	11.701	11.305	...	0.6	0.5	0.4	...
ISOY_053504.87−052057.5	16.334	13.455	10.665	10.271	0.95	0.65	0.22		8.22 ± 1.23
ISOY_053504.90−053949.7	...	15.952	13.007	12.658	...	0.37	0.25	0.2	...
ISOY_053507.53−051114.4	...	12.409	9.991	9.783	...	0.32	0.16	0.13	...
ISOY_053508.07−054853.8	15.701	13.16	9.927	9.45	1.25	1.2	0.18	0.14	7.97 ± 1.59
ISOY_053508.53−052518.0	14.210	12.376	10.231	9.973	1.3	1.07	0.40	0.28	...
ISOY_053508.60−052619.4	11.956	13.274	11.03	10.68	0.25	0.18	0.1	0.1	...
ISOY_053510.07−051706.8	13.722	14.587	10.752	10.068	1.1	0.8	0.25	0.2	...
ISOY_053510.19−052021.0	11.58	13.571	10.938	10.642	0.6	0.45	0.15	0.11	...
ISOY_053510.94−043957.6	...	13.636	11.342	11.075	...	1.25	0.3	0.3	...
ISOY_053510.99−051521.8	...	16.255	9.17	8.561	...	1.7	0.6	0.35	11.29 ± 0.56
ISOY_053516.33−051538.0	...	11.961	9.617	9.354	...	0.6	0.23	0.20	...
ISOY_053516.74−052020.0	...	13.275	9.621	9.34	...	0.8	0.2	0.18	...
ISOY_053518.42−044000.2	...	13.522	12.018	11.67	...	0.28	0.12	...	...
ISOY_053518.70−051801.8	12.457	13.932	10.153	9.85	0.7	1.1	0.4	0.4	7.37 ± 0.80
ISOY_053523.98−052509.8	10.991	13.227	10.6	9.774	0.35	0.35	0.17	0.11	...
ISOY_053524.14−044930.3	...	13.941	11.904	11.515	...	0.79	0.46	0.44	...
ISOY_053525.51−054544.8	14.306	12.887	9.816	9.38	1.6	1.25	0.30	0.25	7.57 ± 0.31
ISOY_053526.73−051645.1	11.22	13.185	11.006	10.806	1.1	0.6	0.26	0.24	2.96 ± 0.62
ISOY_053529.03−050604.1	...	11.675	10.797	10.802	...	0.24	0.06	0.06	...
ISOY_053530.45−052811.3	12.139	13.72	11.575	11.179	0.46	0.22	0.12	0.10	...
ISOY_053534.41−051838.6	...	15.817	11.332	10.781	...	1.15	0.50	0.37	4.75 ± 0.33
ISOY_053535.61−053908.1	15.154	13.793	11.142	10.653	1.25	1.15	0.6	0.5	...
ISOY_053536.42−050115.5	...	10.665	8.632	8.355	...	0.69	0.15	0.14	...
ISOY_053547.65−053738.8	...	12.808	10.413	10.068	...	0.95	0.3	0.25	...
ISOY_053556.10−052533.0	...	15.613	12.045	11.727	...	0.8	0.35	0.26	5.17 ± 0.15
ISOY_053558.94−053253.9	...	14.063	11.466	10.99	...	1.05	0.45	0.42	...

Notes.
[a] ISOY stands for Initial *Spitzer* Orion YSO.
[b] Dip depths are mean values for sources with more than one dip.

Our interpretation is that these objects are being extincted by either "clouds" of relatively higher opacity in the disk atmosphere or geometric warps in the inner disk. In either case the dips are caused as the feature passes through our line of sight to the star as the disk rotates. This hypothesis is consistent with both the event duration and the variation of dip amplitude with wavelength. Further, as some of the dips are periodic or semi-periodic, we note that the derived periods are consistent with those expected from an inner disk region in co-rotation with a star having typical rotation rates for a Class II star (2–14 days). Similar features located further out in the disk could be responsible for the non-repeating and/or broader dips.

As an example, for a period of $P = 8$ days, the "cloud," a region of enhanced dust column density, should be located at a Keplerian orbital radius 0.07 AU (or 7 R_*, for a typical 1 Myr M2 star; Baraffe et al. 1998) and for $P \geqslant 40$ days (i.e., objects showing just one event), the occulting source would be located further than 0.19 AU (or 18 R_*). We can roughly estimate the size and mass of the clouds by using the depth of the events, duration, and standard extinction law. Thus, for an object like that in Figure 3(f), with $P \sim 8$ days and dip duration $\sim$2 days, the size of the occulting body would be about 12 R_*. This large size is better associated with the warped disk model than with a discrete cloud in the disk. Given the average J-band depth of $\sim$1 mag, for the narrowest dips (i.e., dip duration $\sim$12 hr), the occulting body must have a radius >0.6 R_*. If we consider the cloud as a clump of dust grains, we could estimate its mass using the N(H) to A_v relation from Gagne et al. (1995). If the cloud had a radius $\sim$1 R_*, its mass would be $\sim 2 \times 10^{18}$ g. If the cloud were as large as 5 R_*, then the mass of the cloud increases to $\sim 2.5 \times 10^{20}$ g. These masses are small relative to the Moon

($\mathrm{Mass_{Moon}} = 7.35 \times 10^{25}$ g); hence, these clouds are probably not the source material to form a planet.

A problem with the disk obscuration interpretation arises if the flux dips are seen in diskless WTTs. Indeed, there are three ONC members not previously known to have IR excesses (SOY 053524.15−044930.1, SOY 053529.02−050604.0, and SOY 053516.74−052019.7; see Table 6) which have apparent AA-Tau-type flux dips. The two first stars show just one apparent flux dip; the third shows five dips with no clear period. Examination of the spectral energy distributions of these stars shows that the latter shows evidence of having an IR excess at 5.8 and 8 μm (though not at 3.6 and 4.5 μm), consistent with it having a disk with a large inner hole. In this scenario, if the inner disk edge is sufficiently far from the star, there could be no excess at <5 μm, but there still could be material which could occult our view of the star and cause a flux dip. The other two stars could have even larger inner disk holes.

5. CONCLUSIONS

The YSOVAR Orion data provide the first large-scale survey of the photometric variability of YSOs in the mid-IR. In Fall 2009, *Spitzer*/IRAC observed at 3.6 and 4.5 μm a 0.9 deg^2 area centered on the Trapezium cluster twice a day for 40 consecutive days, producing light curves for 1249 known disked YSOs and ∼820 young but generally diskless WTTs, with typical accuracies ∼3%. These data are publicly accessible through the YSOVAR Web site (http://ysovar.ipac.caltech.edu/) or in Table 2.

We find that 70% of the disked YSOs and 44% of the WTTs are variable. The WTT variations are mostly spot-like, while there is a wide range of variability types for the YSOs. Accordingly, 79% of the variable WTTs are periodic, while periods are detected for only 24% of the YSOs. In Table 4 we list 150 new periods found based on these data. We identify five new PMS eclipsing binary candidates, including one already known spectroscopic binary, Theta Ori E, and another one that is fainter than all previously known ONC PMS eclipsing binaries. Coordinates and preliminary periods for the four new eclipsing binary candidates are given in Table 5.

We have discussed in detail a sample of the Orion variables that show short duration flux dips (AA-Tau events). The mean magnitudes of these stars plus the depth of the dips and periods are given in Table 6. We interpret these events as the star being extincted by either clouds of relatively higher opacity in the disk atmosphere or geometric disk warps of relatively higher latitude which pass through the line of sight of the star. This hypothesis is consistent with both the duration and the wavelength-dependent behavior of the events.

We thank the anonymous referee for her helpful comments. This work is based on observations made with the *Spitzer Space Telescope*, which is operated by the Jet Propulsion Laboratory, California Institute of Technology under a contract with NASA. This work is also based (in part) on observations obtained with WIRCam, a joint project of CFHT, Taiwan, Korea, Canada, France, and the Canada–France–Hawaii Telescope (CFHT) which is operated by the National Research Council (NRC) of Canada, the Institute National des Sciences de l'Univers of the Centre National de la Recherche Scientifique of France, and the University of Hawaii.

Facility: Spitzer (IRAC)

REFERENCES

Alencar, S. H. P., et al. 2010, A&A, 519, 88
Anathpindika, S., & Whitworth, A. P. 2008, A&A, 487, 605
Attridge, J. M., & Herbst, W. 1992, ApJ, 398, L61
Baraffe, I., Chabrier, G., Allard, F., & Hauschildt, P. H. 1998, A&A, 337, 403
Bertout, C. 2000, A&A, 363, 984
Bouvier, J., et al. 2003, A&A, 409, 169
Cargile, P. A., Stassun, K. G., & Mathieu, R. D. 2008, ApJ, 674, 329
Carpenter, J. M., Hillenbrand, L. A., & Skrutskie, M. F. 2001, AJ, 121, 3160
Choi, P. I., & Herbst, W. 1996, AJ, 111, 283
Costero R., Allen C., Echevarria J., Georgiev L., Poveda, A., & Richer, M. G. 2008, RevMexAC, 34, 102
Fazio, G. G., et al. 2004, ApJS, 154, 10
Fedele, D., van den Ancker, M. E., Petr-Gotzens, M. G., & Rafanelli, P. 2007, A&A, 472, 207
Fűrész, G., Hartmann, L. W., Megeath, S. T., Szentgyorgyi, A. H., & Hamden, E. T. 2008, ApJ, 676, 1109
Gagne, M., Caillault, J., & Stauffer, J. R. 1995, ApJ, 445, 280
Getman, K. V., Feigelson, E. D., Grosso, N., McCaughrean, M. J., Micela, G., Broos, P., Garmire, G., & Townsley, L. 2005, ApJS, 160, 353
Gutermuth, R. A., Megeath, S. T., Myers, P. C., Allen, L. E., Pipher, J. L., & Fazio, G. G. 2009, ApJS, 184, 18
Haro, G. 1969, Bol. Obs. Tonantzintla Tacubaya, 5, 79
Herbig, G. H., & Griffin, R. F. 2006, AJ, 132, 1763
Herbig, G. H., & Kameswara Rao, N. 1972, ApJ, 174, 401
Herbst, W., Bailer-Jones, C. A. L., Mundt, R., Meisenheimer, K., & Wackermann, R. 2002, A&A, 396, 513
Herbst, W., Herbst, D. K., Grossman, E. J., & Weinstein, D. 1994, AJ, 108, 1906
Herbst, W., LeDuc, K., Hamilton, C. M., Winn, J. N., Ibrahimov, M., Mundt, R., & Johns-Krull, C. M. 2010, AJ, 140, 2025
Hillenbrand, L. A., Carpenter, J. M., & Skrutskie, M. F. 2001, ApJ, 547, L53
Hillenbrand, L. A., Strom, S. E., Calvet, N., Merrill, K. M., Gatley, I., Makidon, R. B., Meyer, M. R., & Skrutskie, M. F. 1998, AJ, 116, 1816
Irwin, J., et al. 2007, MNRAS, 380, 541
Johnson, J. J., Gehrz, R. D., Jones, T. J., Hackwell, J. A., & Grasdalen, G. L. 1990, AJ, 100, 518
Jones, B. F., & Walker, M. F. 1988, AJ, 95, 1755
Kovács, G., Zucker, S., & Mazeh, T. 2002, A&A, 391, 369
McNamara, B. J. 1976, AJ, 81, 845
Parenago, P. P. 1954, Tr. Gos. Astron. Inst., 25, 1
Parsamian, E. S., Chavira, E., & González, G. 1993, RevMexAA, 25, 71
Plavchan, P., Gee, A. H., Stapelfeldt, K., & Becker, A. 2008a, ApJ, 684, L37
Plavchan, P., Jura, M., Kirkpatrick, J. D., Cutri, R. M., & Gallagher, S. C. 2008b, ApJS, 175, 191
Rayner, J., McLean, I., Aspin, C., & McCaughrean, M. 1989, MNRAS, 241, 469
Rebull, L. M. 2001, AJ, 121, 1676
Reipurth, B., Rodríguez, L. F., & Chini, R. 1999, AJ, 118, 983
Scargle, J. D. 1982, ApJ, 263, 835
Stassun, K. G., Mathieu, R. D., Mazeh, T., & Vrba, F. J. 1999, AJ, 117, 2941
Stassun, K. G., Mathieu, R. D., & Valenti, J. A. 2006, Nature, 440, 311
Stassun, K. G., Mathieu, R. D., Vaz, L. P. R., Stroud, N., & Vrba, F. J. 2004, ApJS, 151, 357
Takahashi, S., Saito, M., Ohashi, N., Kusakabe, N., Takakuwa, S., Shimajiri, Y., Tamura, M., & Kawabe, R. 2008, ApJ, 688, 344
Tian, K. P., van Leeuwen, F., Zhao, J. L., & Su, C. G. 1996, A&AS, 118, 503
Tobin, J. J., Hartmann, L., Furesz, G., Mateo, M., & Megeath, S. T. 2009, ApJ, 697, 1103
Walker, M. F. 1978, ApJ, 224, 546
Welch, D. L., & Stetson, P. B. 1993, AJ, 105, 1813
Werner, M. W., et al. 2004, ApJS, 154, 1
Yu, K. C., Bally, J., & Devine, D. 1997, ApJ, 485, L45